**Pure and Applied Geophysics**

CrossMark

# Ionospheric Plasma Response to $M_w$ 8.3 Chile Illapel Earthquake on September 16, 2015

C. D. Reddy,[1] Mahesh N. Shrivastava,[2,3] Gopi K. Seemala,[1] Gabriel González,[2,3] and Juan Carlos Baez[4]

*Abstract*—The lithosphere and the atmosphere/ionosphere continuously exchange energy through various coupling mechanisms. In particular, the earth surface displacement caused by earthquakes, volcanoes and tsunamis can manifest as ionospheric plasma perturbations. We investigate the coseismic induced ionospheric total electron content (TEC) perturbations following the $M_w$ 8.3 Illapel thrust earthquake that occurred on September 16, 2015. The continuous global positioning system (GPS) data at 48 sites from Centro Sismológico Nacional and International GNSS Service GPS networks have been used in this study. The nearest GPS site recorded the ionospheric response 10 min after the occurrence of this earthquake. The maximum vertical coseismic induced TEC amplitude is $\sim$1.4 TECU, and the perturbations are pronounced in the northern region of the epicenter and confined to less than $\sim$1500 km radius. The average horizontal acoustic wave velocity has been determined as $\sim$1260 m/s. We also observed acoustic resonance recorded by PRN 12 at 4.3 mHz corresponding to the first overtone of acoustic mode and lasting for about 30 min. In this study, we present characteristics of GPS derived ionospheric plasma perturbations following Illapel earthquake.

**Key words:** GPS TEC, Illapel earthquake, coseismic, ionosphere, plasma, acoustic resonance.

## 1. Introduction

The earth is surrounded by atmosphere whose layers are troposphere, stratosphere, mesosphere and thermosphere. The ionosphere (ionized region of thermosphere) is the part of the earth's atmosphere located around 100–1000 km altitude that contains ionized gas, called plasma, which influences the radio wave propagation. Ionospheric disturbances are caused from sources located above it, e.g. the sun, interplanetary medium, magnetosphere, and below it, e.g. mesosphere, stratosphere, troposphere and lithosphere. Lithospheric disturbances are mainly due to earthquakes, volcanic eruptions, cryospheric or human activity (e.g. nuclear explosions). Following an earthquake, the ionosphere is mainly disturbed by shock acoustic waves, Rayleigh wave induced acoustic waves and tsunami induced gravity waves whose frequencies fall between 0.1 and 10 mHz. Detecting these seismo-ionospheric signals turns out to offer a possible remote sensing of seismic signals (Lognonné et al. 2006) mainly for the two reasons (1) by continuity of vertical displacement at the surface, the atmosphere is then forced to move with the same vertical velocity as the ground surface and (2) conservation of kinetic energy and the exponential decrease of air density with the height. Further, it should be noted that it is easier to detect waves propagating in ionospheric plasma, more than in neutral atmosphere because of the radio-propagation properties (dispersive nature) of plasma.

The recent technological advances colossally facilitating the monitoring the seismo-ionospheric perturbations with both ground and space based advanced radio techniques. HF Doppler sounding (Liu et al. 2006; Artru et al. 2004; Ogawa et al. 2012), DEMETER (Liu et al. 2015), Over-The-Horizon radar (Occhipinti et al. 2010), and GPS (Ducic et al. 2003; Heki 2011; Reddy et al. 2015) are some of the well-established techniques for monitoring ionospheric plasma perturbations caused by large earthquakes. In particular, the GPS receivers are very handy and affordable and provide integrated total electron content (TEC). The integrated value is called total electron content (TEC) and defined as 1 TECU = $10^{16}$ ele/m$^2$. GPS-based ionospheric

[1] Indian Institute of Geomagnetism, Navi Mumbai, India. E-mail: cdreddy@iigs.iigm.res.in
[2] National Research Center for Integrated Natural Disaster Management, Santiago, Chile.
[3] Universidad Católica del Norte, Antofagasta, Chile.
[4] Centro Sismológico Nacional, Universidad de Chile, Santiago, Chile.

Table 1

*Parameters of earthquakes of different severity in Chile region (Great Chilean Earthquake; Maule earthquake; Pisagua Earthquake; Illapel Earthquake)*

| Chile events | Date | Time (UT) | Longitude | Latitude | $M_w$ | Depth (km) | Fault | TECU | References |
|---|---|---|---|---|---|---|---|---|---|
| Great Chilean | 22.05.1960 | 19:11 | 287.00E | 38.23S | 9.5 | 33 | Thrust | – | No GPS-TEC |
| Maule | 27.02.2010 | 06:34 | 287.10E | 36.12S | 8.8 | 23 | Thrust | 0.1–0.2 | GALVAN et al. (2011) |
| Maule | 27.02.2010 | 08:01 | 284.59E | 38.09S | 7.4 | 20 | Thrust | 0.1–0.2 | GALVAN et al. (2011) |
| Pisagua | 01.04.2014 | 23:46 | 285.50E | 19.61S | 8.1 | 25 | Thrust | 1.25 | REDDY et al. (2015) |
| Illapel | 16.09.2015 | 22:54 | 288.33E | 31.57S | 8.3 | 33 | Thrust | 1.4 | Present study |

measurement can measure TEC variations smaller than 0.01 TECU (DUCIC et al. 2003).

It should be kept in mind that, in addition to the above mentioned seismic sources (e.g., earthquakes and volcanoes), explosions, e.g., nuclear, chemical (ROW 1967), rocket and space shuttle launching (DING et al. 2014; CALAIS and MINSTER 1996), ballistic missiles (OZEKI and HEKI 2010), and even asteroids and surface mine blasts, generate significant ionospheric perturbations (CALAIS and MINSTER 1996). Solar events (e.g., coronal mass ejections and solar flares), atmospheric phenomena (e.g., thunderstorms and lightning), and meteorological events (e.g., typhoons and tornadoes) (HUANG et al. 1985; BISHOP et al. 2006) remain main sources of ionospheric perturbations.

It is demonstrated that dense GPS arrays such as Southern California Integrated GPS Network (SCIGN) (CALAIS et al. 2003), Japanese GPS Earth Observation Network (GEONET, operated by GSI, Japan, (SAGIYA 2004; OGAWA et al. 2012; SAITO et al. 2001) Sumatra GPS Array (SuGAr), Integrated Plate boundary Observatory Chile (IPOC) (REDDY et al. 2015), Indian Seismic and GPS Network (ISGN) (REDDY and SEEMALA 2015), etc. provide an opportunity to investigate ionospheric perturbations and their spatio-temporal characteristics. The imaged ionospheric perturbations from dense GPS arrays could, in principle, be used as a proxy to study the coupling and energy transfer processes in the lithosphere, atmosphere and ionosphere (LAI) coupled system (CALAIS et al. 2003).

Subduction zones are plate tectonic boundaries where two plates converge, and one plate is thrust beneath the other resulting large to mega earthquakes and volcanoes. In particular, in Chile subduction region many earthquakes with different severity recorded by seismometers in last four decades

(Table 1). Geophysicists and seismologists try to understand physics of the mega thrust earthquake processes, to facilitate seismic hazard mitigation. Ionospheric seismologists are doing their part to supplement to this understanding from seismo-ionospheric manifestations. An earthquake of $M_w$ 8.3 struck on September 16, 2015; 24 km west of Chile's coast, generating strong ground shaking, permanent crustal deformation, free oscillations of the earth and triggering a tsunami. This study mainly pertains to investigating the imprint of this earthquake in ionospheric plasma (henceforth referred as ionospheric perturbation) from the analysis of GPS data.

## 2. Seismo-Tectonics of Chile Subduction Zone

The Chilean western coast is characterized by subduction of the Nazca plate underneath the South American plate, resulting in frequent, large interplate earthquakes. In the northern segment of the Chile subduction zone, the convergence between both plates is taking place in east–northeast direction at a rate of 66 mm/year (MÉTOIS et al. 2013). Several earthquakes with magnitude >7.5 have occurred at the plate interface between the subducting Nazca and the overriding South American plates during the 20th and 21st centuries. This historical record of seismicity shows that the largest earthquake recorded to date is the 1960 $M_w$ 9.5 Valdivia earthquake. The slip deficit accumulated along the central and northern segments of the Chilean subduction zone has allowed to define at least three major seismic gaps (CHLIEH et al. 2011; SCHURR et al. 2014). Two of these seismic gaps have already released the accumulated slip deficit during the past 2 years.

## 2.1. $M_w$ 8.3 Illapel Earthquake

The $M_w$ 8.3 interplate thrust earthquake occurred at 22:54 h on September 16, 2015, rupturing offshore Illapel, Chile, producing a local tsunami of 4.7 m height. The earthquake located on the primary plate boundary interface between Nazca and South America plates (shown as star in Figs. 1, 2), and occurred as a consequence of the convergence of the Nazca plate and South America plate that actuated at rate of 66 mm/year (ANGERMANN et al. 1999). Broadband seismic data
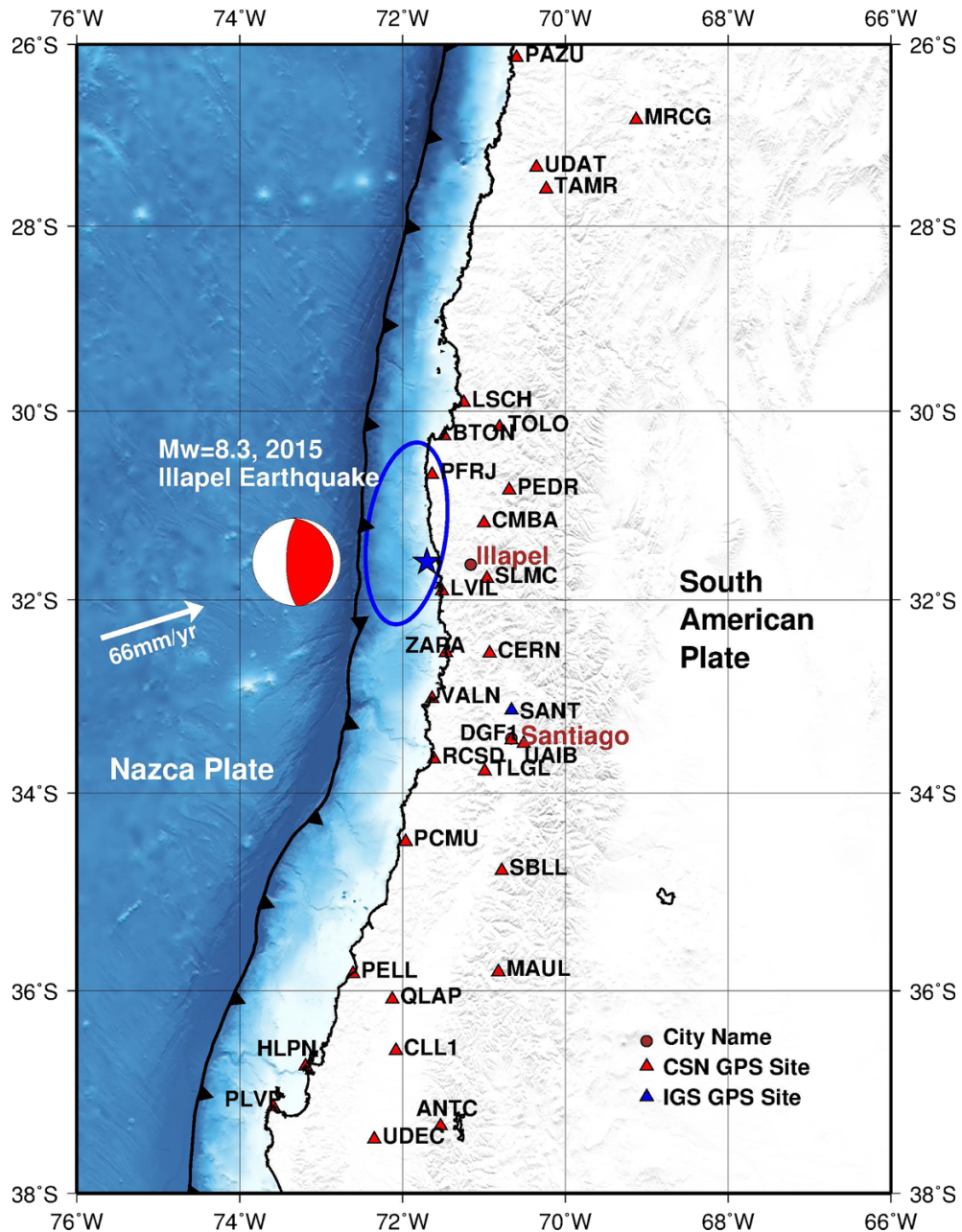


Figure 1
The *blue star* indicates the location of the $M_w$ 8.3 Illapel thrust earthquake on September, 2015. The network of CSN GPS sites (*red triangle*) and IGS (*blue triangles*). The *blue ellipse* indicates the ruptured area of the Illapel earthquake
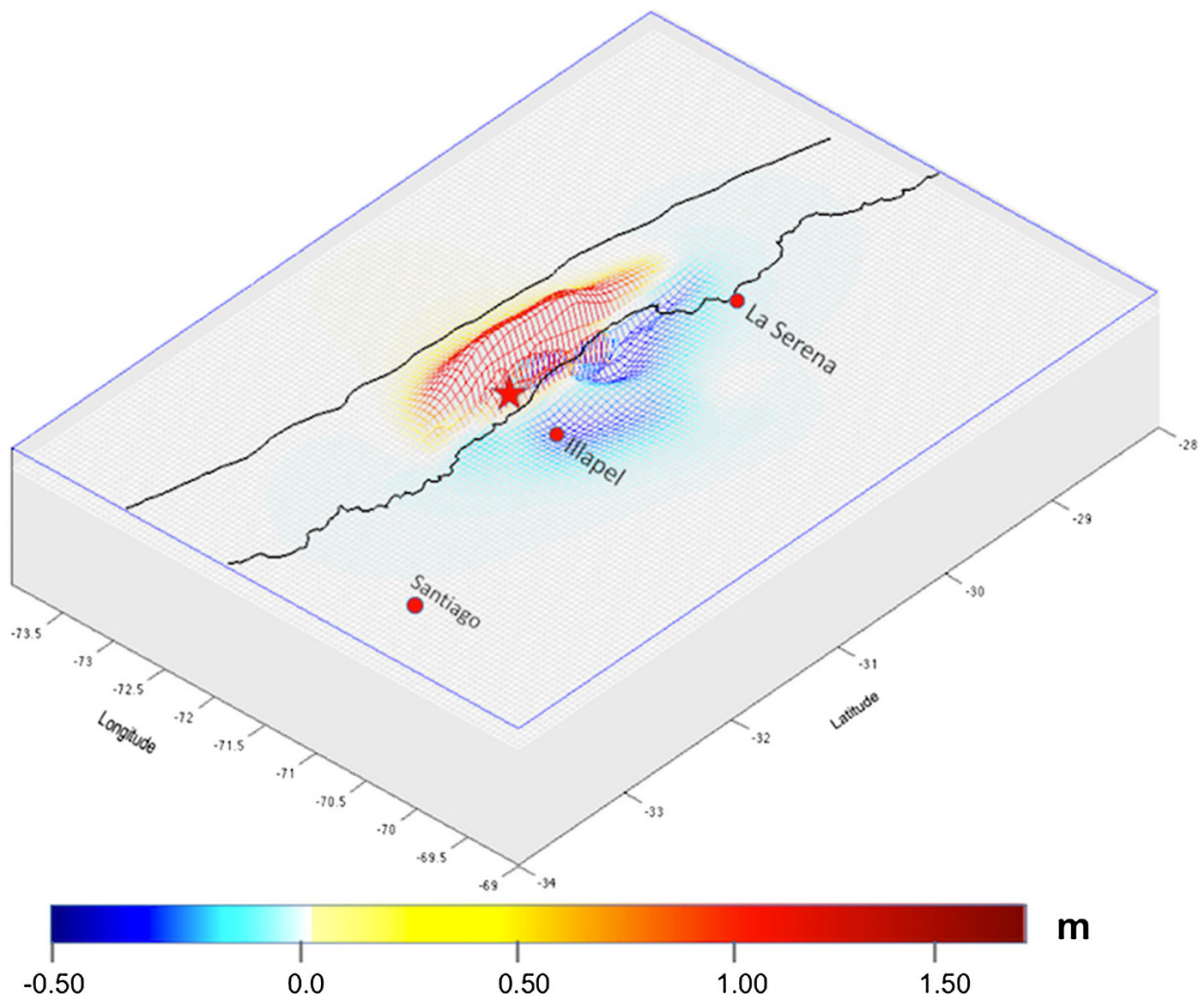
Figure 2
Modeled vertical deformation due to $M_w$ 8.3 Illapel thrust earthquake on September 16, 2015. The *star* indicates location of the earthquake. Maximum vertical displacement of 1.78 m and subsidence of 0.46 m is simulated

indicated northward rupture expansion from the hypocenter with a rupture velocity of 1.5–2.0 km/s and 180–240 km along-strike rupture with peak of slip of 7–10 m (Ye *et al.* 2015). The estimated seismic moment $3.7 \times 10^{21}$–$2.7 \times 10^{21}$ N m with static stress drop estimates range from 2.6 to 3.5 MPa, and the radiated seismic energy, up to 1 Hz, is about $2.2$–$3.15 \times 10^{16}$ J.

### 2.2. Vertical Deformation of Illapel Earthquake

The coseismic slip of Illapel earthquake has been inverted from GPS displacements using a damped linear least squares inversion based on Green's

functions generated with a Finite Element model. This coseismic slip model is used for vertical displacement computation. The Coulomb 3.1 program (Toda *et al.* 2005; Lin and Stein 2004) is used to estimate the coseismic vertical deformation for a given fault geometry and the coseismic slip. In this analysis, we have considered the Poisson's ratio 0.25 and an effective coefficients of friction, $\mu = 0.6$. The vertical deformation provided by slip considering a finite rectangular source embedded in an elastic, homogeneous and isotropic half space (Okada 1992). The GPS sites recorded subsidence and westward motion around the rupture area, with a maximum of 0.40 and 1.45 m, respectively. The stimulated

maximum vertical uplift off coast is around 1.78 m and subsidence in the coast around 0.43 m.

### 3. GPS Data Analysis

We utilized the GPS data from 48 permanent sites (aeda, antc, arjf, bton, cern, chyt, cll1, cmba, crsc, csom, dgf1, futf, glps, hlpn, iqqe, ispa, lnqm, lsch, lvil, maul, mrcg, navi, pazu, pcmu, pedr, pell, pfrj, plvp, ptro, qlap, qlln, rado, rcsd, sant, sbll, slmc, spat, tamr, tlgt, tmco, tolo, uaib, udat, udec, utar, valn, vohg, zapa) which are part of CSN (43 stations) and IGS (five stations—antc, glps, iqqe, sant and ispa) networks (shown in red and blue triangles in Fig. 1), which forms an excellent GPS data set to study the near field earthquake induced ionospheric perturbations. However, we have shown only few stations in Fig. 1, leaving aside far away stations, which have not shown significant response in ionosphere. All these sites provide the GPS data sampled at 30 s interval.

The calculation of the ionospheric vertical TEC was done independently at all these sites using both code and phase measurements of the two, i.e., $L_1$ ($f_1 = 1575.42$ MHz) and $L_2$ ($f_2 = 1227.60$ MHz) frequencies. Thus, we eliminated the effect of clock errors and tropospheric water vapor and estimated the relative values of slant TEC (Sardón and Zarraoa 1997). Then, the absolute values of TEC are obtained by including the differential satellite biases published by the University of Bern and the receiver bias that is calculated by minimizing the TEC variability between 02:00 and 06:00 LT (Valladares et al. 2009; Seemala and Valladares 2011).

It is important to note that the presence of horizontal electron density gradients in the ionosphere cause STEC to VTEC conversion errors using thin shell approximation mapping function (Nava et al. 2007) and are pronounced at lower elevation angles. But, when it is required to compare the signature in TEC, the lower the elevation angle, the higher the signature is amplified and may be more contaminated with other effects ex: multipath, tropospheric scatter. Therefore, to compare the signature of seismic origin for TEC at higher elevation angles to lower elevation angles, the STEC is converted to VTEC using a simple mapping function which normalizes the amplitudes for all elevation angles except at acute angles. In this study, we expect that 5–10 % conversion error in TEC amplitude, while other response characteristics remain unaffected.

Thus, estimated TEC can have high degree of accuracy, i.e., at least $10^{14}$ ele/m$^2$ at 30 s sampling rate (in this study the GPS data are considered sampled at 30 s interval). Short-term ionospheric perturbations are extracted by applying a band-pass filter 2–10 milli-Hertz (mHz). For representation purpose, we locate the TEC measurement at the intersection of the line of sight and an ionospheric thin layer, whose altitude is chosen near the peak of electron density. In this analysis we have considered the height of the ionospheric thin shell at 350 km. These points are referred to as ionospheric piercing points (IPPs). As the GPS TEC technique is strongly dependent on the observation geometry, we considered the geometries for several satellites, viz., PRN 12, PRN 24 and PRN 25. Figure 3 gives the ionospheric response at various continuous GPS sites. As seen in Fig. 3, following the 2015 Illapel earthquake, we observed that maximum coseismic ionospheric response is as large as $\sim$1.4 TECU (peak to peak) at station pazu located north of epicenter $\sim$610 km away.

It should be noted that such TEC magnitude can be caused by variety of sources (Pulinets 2004). At times, it is feasible to use geomagnetic (Kp, Ap, and Dst), solar (F10.7) and ionospheric scintillation (S4, and $\sigma\varphi$) indices to distinguish seismo-ionospheric anomalies from that of geomagnetic, solar and ionospheric disturbances. September 16, 2015 was a geomagnetically quiet day ($K_p = 2$). However, the best way to check that the observed plasma perturbation is caused by, e.g. shock acoustic waves, Rayleigh wave or tsunami induced is using hodochron plots (travel-time plots) generated for all the PRNs (in this study PRN 12, PRN 24 and PRN 25) as shown in Fig. 4, where a clear linear relationship (shown as gray lines) between travel time and epicentral distance. The positive and negative distances indicate North and South directions from the epicenter respectively. Slope of the slant lines give the average horizontal acoustic wave velocities of $\sim$1260 and $\sim$590 m/s in the northern and southern sides respectively.
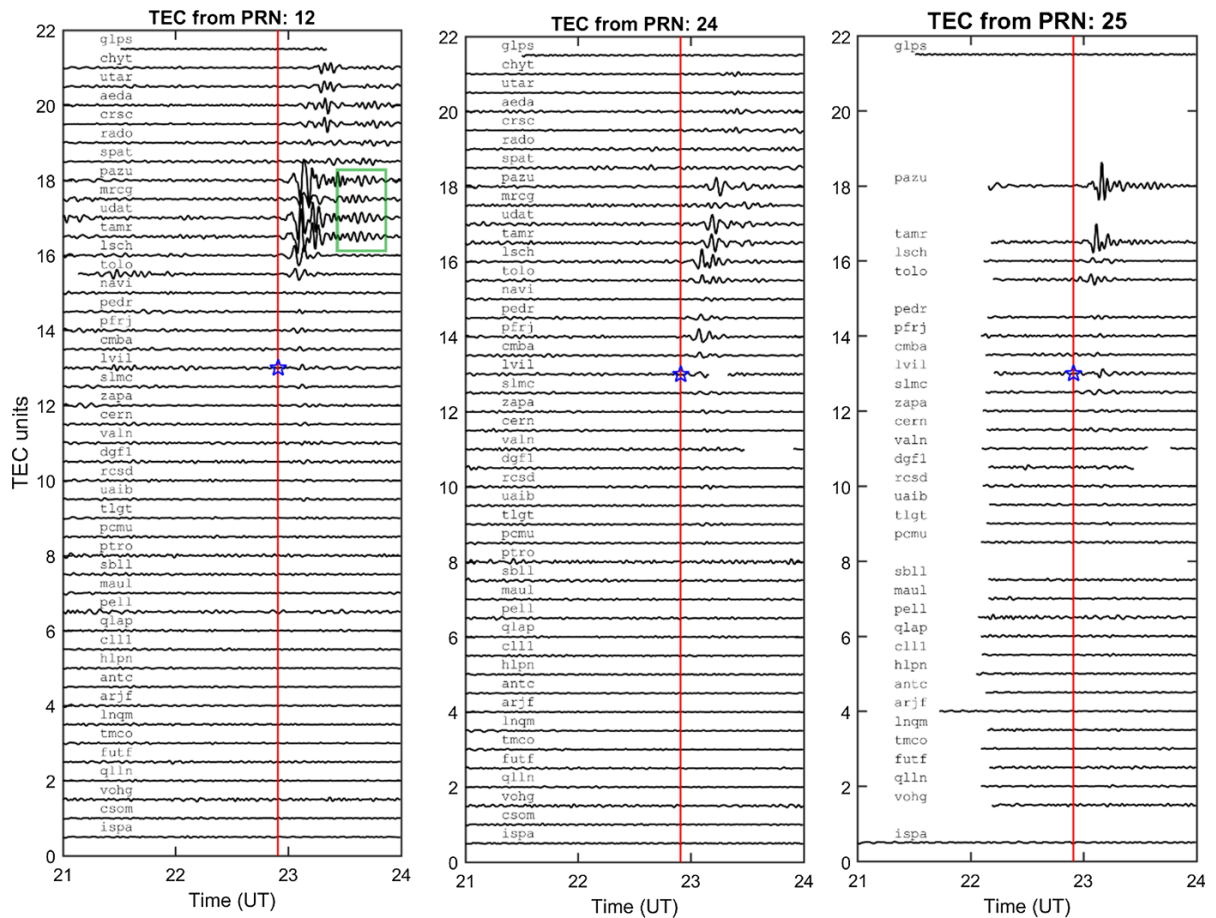
Figure 3
Stacks of vertical TEC variation for PRN 12, 24 and 25 for GPS sites from CSN and IGS GPS networks, for 2 h duration containing the Illapel earthquake event on September 16, 2015. The *red vertical line* indicates the time of the earthquake. The *blue star* on the *red vertical line* indicates the location of the earthquake such that sites north and south of the epicenter can easily noticed. The *green box* in the *left panel* highlights the stations (pazu, udat and tamr) exhibiting the acoustic resonance, also shown in Fig. 5 with wavelet spectral analysis

## 4. Results and Discussion

The $M_w$ 8.3 Illapel earthquake on September 16, 2014, ruptured central Chile subduction zone. As shown in Fig. 2, it caused maximum vertical coseismic displacement of 1.78 m off coast and subsidence of 0.42 m in the land. In this scenario, we can expect ionospheric TEC perturbations from many possibilities (1) acoustic waves of typical sound velocity 500–1500 km/s directly generated by the earthquake itself (HEKI and PING 2005; CALAIS et al. 1998), (2) AGW by surface Rayleigh waves with velocity 2000–4000 m/s and (3) tsunami waves with propagation speed ∼200 m/s (e.g. MARUYAMA et al. 2011;

TSAI et al. 2011). It should be noted that the focal mechanism of the earthquake, the rupture propagation, magnitude and time of earthquake also plays significant role in manifestation of the ionospheric response (ASTAFYEVA and HEKI 2009). CAHYADI and HEKI (2015) provide scaling law, which represents relation between induced TEC and moment magnitude of the earthquake.

The analysis of the GPS data from 48 GPS sites from CSN and IGS networks indicates a clear northward directivity due to the combined effects of the (1) equator ward geomagnetic field (HEKI and PING 2005; CALAIS et al. 1998), i.e. coupling factor between the neutral wave and the geomagnetic field
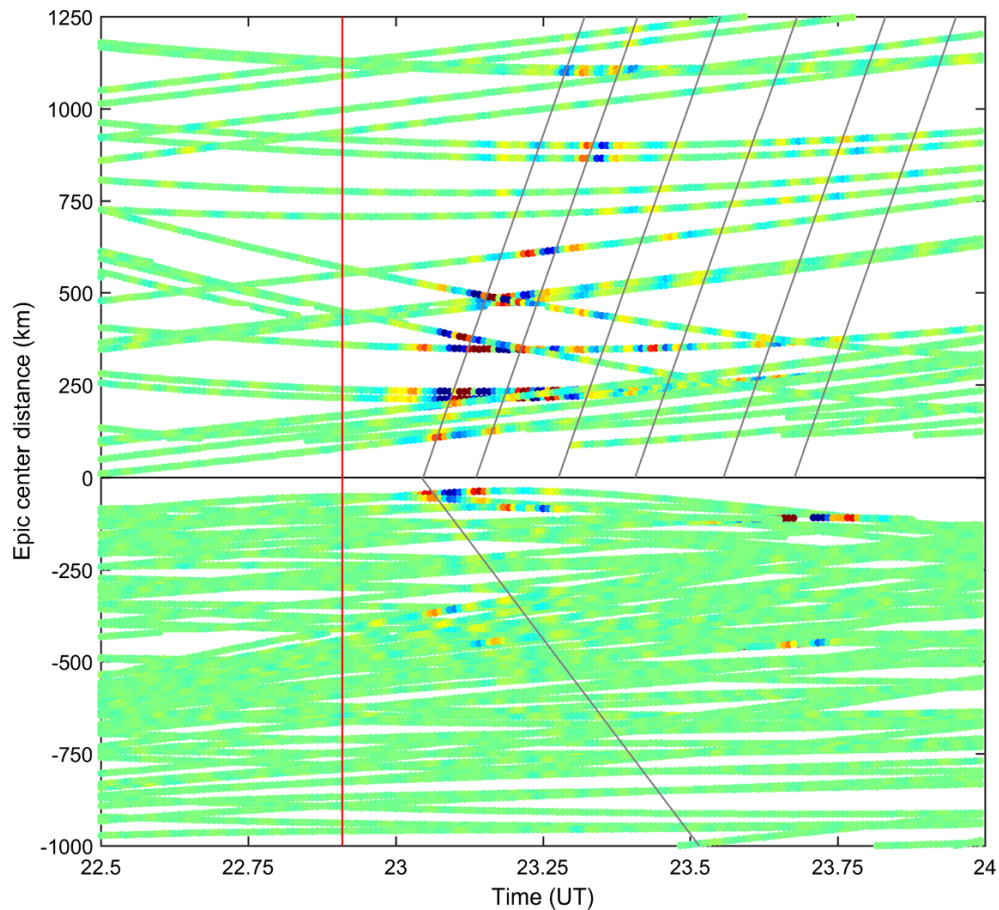
Figure 4
*Hodochron plot* showing variation in vertical TEC at various GPS sites as a function of time and epicentral distance, obtained from PRN 12, 24 and 25. The positive and negative epicentral distances indicate North and South directions from the epicenter respectively. Slope of the northern and southern side slant lines gives the average horizontal velocity of the acoustic wave, estimated as ~1260 and ~590 m/s respectively. The *parallel lines* are drawn to indicate the acoustic resonance at some GPS sites (see Fig. 5)

is proportional to the cosine of the angle enclosed by the geomagnetic field vector and the wave vector, and (2) rupture propagation which is in NNE direction (YE *et al.* 2015) is shown in Fig. 3. Few stations (bton, iqqe, plvp, sant, udec) whose data are not good were excluded from Fig. 3. Further, the characteristics of the wave form and it's amplitude depend on the observation geometry of the GPS satellites (line-of-sights), disturbance wave front (point source/extended source), and azimuth of Sub Ionospheric Point (SIP) relative to epicenter (ASTAFYEVA and HEKI 2009). These characteristics also can vary little with the local time, the season, and the level of geomagnetic disturbance (AFRAIMOVICH *et al.* 2001) as the response time varies from these parameters. It is to be

noted that the level of geomagnetic disturbances was quiet during the Illapel earthquake on September 16, 2015 with $K_p$ index varied from 0 to 2.

It is very conspicuous that the ionospheric plasma perturbations seems to be mainly caused by (1) shock acoustic waves and (2) acoustic resonance due to shock acoustic waves. The ionospheric response is seen after ~10 min delay with respect to the Illapel earthquake time. After reaching the ionospheric height, the perturbation propagated with horizontal velocity of ~1260 m/s and diminishing with epicentral distance. It should be noted that the ionospheric response corroborate with the earthquake rupture and energy dissipation. YE *et al.* (2015), estimated these parameters where it is seen that
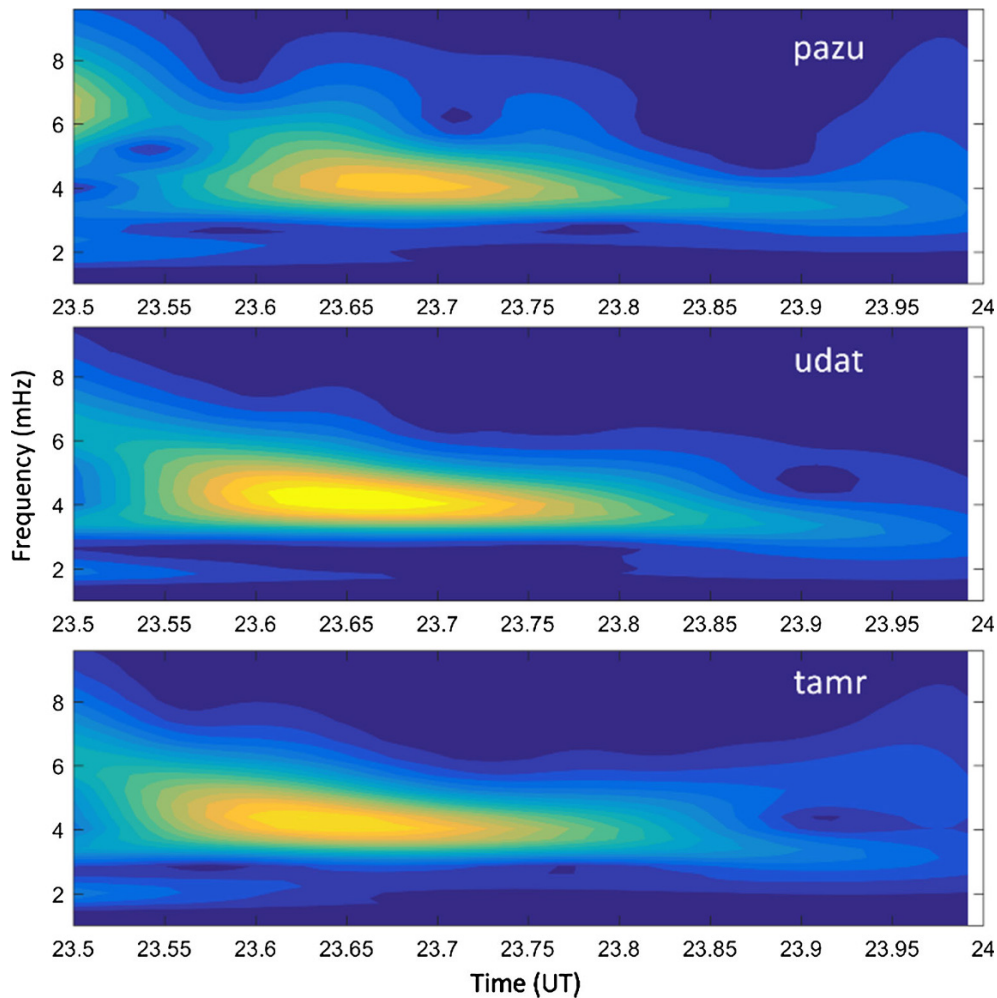
Figure 5
Wavelet spectrograms of vertical TEC time series for GPS sites pazu, udat and tamr. It is clearly evident that acoustic resonance with ~4.3 mHz is seen persisting for about 30 min

maximum earthquake energy is dissipated while the rupture was progressing in NNE direction and located ~200 km from epicenter. Despite this earthquake has higher magnitude, i.e. $M_w$ 8.3 in comparison with Pisagua $M_w$ 8.1 earthquake (REDDY et al. 2015, Table 1), the later has generated wide spread ionospheric response comparing to the Illapel. Where as the Illapel earthquake generated wide spread acoustic resonance as described in the following paragraph.

The resonance is observed at GPS sites tamr, udat, mrcg and pazu (see Fig. 1) that seem to be falling along the line of rupture zone. The wavelet spectral analysis (Fig. 5) shows that this signal is characterized by 4.3 mHz, corresponding to the first

overtone of acoustic atmospheric trapped acoustic mode (LOGNONNÉ et al. 1998; KOBAYASHI 2007). The acoustic resonance lasted for about 30 min, appear to be excited by shock acoustic waves. Also, following 2004 $M_w$ 9.2 Sumatra earthquake, a wave train about 4 h at 3.9 mHz acoustic resonance was observed at phkt, samp, bnkk whose distance from the epicenter was less than 1200 km (CHOOSAKUL et al. (2009). Similar to our study (Illapel earthquake), these sites (except mrcg) also seen located parallel to the rupture faults. It can be hypothesized that the GPS sites over the rupture area may be one of the favourable conditions for the acoustic resonance to observe.

In case of Illapel earthquake, we have observed a train of wave packet of TEC variation, seems resulting from beat of the atmospheric modes around observed resonant frequency 4.3 mHz as explained by DAUTERMANN et al. (2009). Such phenomenon was seen in 2004 Sumatra earthquake and is also consistent with numerical model given by MATSUMURA et al. (2011). Similarly, in the case of (i) the 2011 $M_w$ 9.0 Tohoku-Oki earthquake, the resonance at 3.7 and 4.5 mHz was observed at site, i.e. at 0979 in GEONET (ROLLAND et al. 2011). The former frequency lasted for about 2 h due to the high quality factor. (ii) Following the Mw 8.6 Indian Ocean earthquake, the acoustic resonance at 4.1 mHz observed at the GPS site 'ulmh' from SuGAr GNSS network, which lasted for about 30 min (SUNIL et al. 2015). All the above mentioned resonant frequencies are consistent with the acoustic resonance between the ground and lower thermosphere as predicted by numerical model (SAITO et al. 2011). The long duration of acoustic resonance can be linked to high quality factor with well-defined resonance frequencies, and hence with decreased beat frequency.

It can be observed from Fig. 4 that the acoustic velocity towards north is $\sim 1260$ m/s while it is $\sim 590$ m/s towards south (though it is not very clear signature). One possibility for this discrepancy is that, as shown in the Fig. 1, the rupture area (indicated by blue ellipse) and propagation is in north direction facilitating increased northern horizontal acoustic velocity and decreased southern velocity. It can be verified to some extent if the 1 s GPS data is available. Other remote possibility is that, in southern side those waves are generated by secondary gravity waves produced by primary shock acoustic waves in tropopause, as hypothesized by REDDY et al. (2015).

## 5. Conclusions

We studied the characteristics of ionospheric perturbations induced by shock acoustic waves of $M_w$ 8.3 Illapel earthquake, using continuous GPS data from CSN and IGS networks, demonstrating that such GPS networks are powerful tools in imaging ionospheric perturbations in 2–10 mHz frequency range.

The average velocity of the acoustic wave has been estimated as $\sim 1260$ m/s. The coseismic ionospheric signal with peak-to-peak value of $\sim 1.4$ TECU and confined to less than a radius of $\sim 1500$ km corroboration with the characteristics of shock acoustic waves. Wide spread acoustic resonance was observed at many sites with resonance frequency 4.3 m Hz corresponding to the first overtone of acoustic mode and lasting for about 30 min. As the signal was feeble, it was difficult to discern the ionospheric TEC perturbations caused by Rayleigh or/and tsunami.

## REFERENCES

AFRAIMOVICH E. L, PEREVALOVA N. P., PLOTNIKOV A. V., URALOV A. M., (2001), *The shock-acoustic waves generated by the earthquakes.* Ann. Geophys., *19*(4), 395–409.

ANGERMANN D., KLOTZ J., REIGBER C., (1999), *Space-geodetic estimation of the Nazca- South America Euler vector.* Earth Planet Sci. Lett., *171*, 329–334.

ARTRU J., FARGES T., LOGNONNE P., (2004), *Acoustic waves generated from seismic surface waves: Propagation properties determined from Doppler sounding observations and normal-mode modeling.* Geophys. J. Int., *158*, 1067–1077.

ASTAFYEVA, E., and HEKI, K., (2009), *Dependence of wave form of near-field coseismic ionospheric disturbances on focal mechanisms.* Earth Planet Space, *61*, 939–943.

BISHOP, R. L., N. APONTE, G. D. EARLE, M. SULZER, M. F. LARSEN, and G. S. PENG (2006), *Arecibo observations of ionospheric perturbations associated with the passage of Tropical Storm Odette*, J. Geophys. Res., *111*, A1132, doi:10.1029/2006JA011668.

CAHYADI, M. N., and K. HEKI (2015), *Coseismic ionospheric disturbance of the large strike-slip earthquakes in North Sumatra in 2012: Mw dependence of the disturbance amplitudes*, Geophys. J. Int., *200*, 116–129.

CALAIS E., MINSTER J.B., (1996), *GPS detection of ionospheric perturbations following a Space Shuttle ascent.* Geophys. Res. Lett., *23*, 1897–1900.

CALAIS E., MINSTER J. B., HOFTON M., HEDLIN M., (1998), *Ionospheric signature of surface mine blasts from Global Positioning System measurements.* Geophys. J. Int., *132*, 191–202.

CALAIS E., HAASE J. S., MINSTER J.B., (2003), *Detection of ionospheric perturbations using a dense GPS array in Southern California*. Geophys. Res. Lett., *30*(12), 628, doi:10.1029/2003GL017708.

CHLIEH M., et al., (2011), *Interseismic coupling and seismic potential along the Central Andes subduction zone*. J. Geophys. Res., *116*, B12405, doi:10.1029/2010JB008166.

CHOOSAKUL, N., A. SAITO, T. IYEMORI, and M. HASHIZUME, (2009), *Excitation of four minute periodic ionospheric variations following the great Sumatra-Andaman earthquake in 2004*, J. Geophys. Res., *114*, A10313, doi:10.1029/2008JA013915.

DAUTERMANN, T., E. CALAIS, P. LOGNONNÉ, and G. S. MATTIOLI (2009), *Lithosphere–atmosphere–ionosphere coupling after the 2003 explosive eruption of the Soufriere Hills Volcano, Montserrat*, Geophys. J. Int., *179*, 1537–1546, doi:10.1111/j.1365-246X.2009.04390.x.

DING F., WAN W., MAO T., WANG M., NING B., ZHAO B., XIONG B., (2014), *Ionospheric response to the shock and acoustic waves excited by the launch of the Shenzhou 10 spacecraft*. Geophys. Res. Lett., *41*, 3351–3358, doi:10.1002/2014GL060107.

DUCIC V., ARTRU J., LOGNONNE P., (2003), *Ionospheric remote sensing of the denali earthquake rayleigh surface waves*. Geophys. Res. Lett., *30*(18), 1951–1954.

GALVAN D. A., KOMJATHY A., HICKEY M. P., MANNUCCI A.J., (2011), *The 2009 Samoa and 2010 Chile tsunamis as observed in the ionosphere using GPS total electron content*. J. Geophys. Res., *116*, A06318, doi:10.1029/2010JA016204.

HEKI K., (2011), *Ionospheric electron enhancement preceding the 2011 Tohoku-Oki earthquake*. Geophys. Res. Lett., *38*, L17312, doi:10.1029/2011GL047908.

HEKI K. and PING J., (2005), *Directivity and apparent velocity of the coseismicionospheric disturbances observed with a dense GPS array*. Earth Planet Sci. Lett., *236*, 845–855, doi:10.1016/j.epsl.2005.06.010.

HUANG, Y. N., C. KANG, and S. W. CHEN (1985), *On the detection of acoustic gravity waves generated by typhoon by use of real time HF Doppler frequency shift sounding system*, Radio Sci., *20*, 897–906, doi:10.1029/RS020i004p00897.

KOBAYASHI, N. A, (2007), *New method to calculate normal modes*, Geophys. J. Int. *168*, 315–331.

LIN J. and STEIN R. S., (2004), *Stress triggering in thrust and subduction earthquakes, and stress interaction between the southern San Andreas and nearby thrust and strike-slip faults*. J. Geophys. Res., *109*, B02303, doi:10.1029/2003JB002607.

LIU J. Y., TSAI Y. B., CHEN S. W., LEE C. P., CHEN Y. C., YEN H. Y., CHANG W. Y., LIU C., (2006), *Giant ionospheric disturbances excited by the M 9.3 Sumatra earthquake of 26 December 2004*. Geophys. Res. Lett., *33*, L02103, doi:10.1029/2005GL023963.

LIU J.Y., CHEN Y.I., HUANG C.C., PARROT M., SHEN X.H., PULINETS S.A., YANG Q.S., HO Y.Y., (2015), *A spatial analysis on seismoionospheric anomalies observed by DEMETER during the 2008 M8.0 Wenchuan earthquake*, Journal of Asian Earth Sciences, *114*, 414–419.

LOGNONNÉ, P., E. CLÉVÉDÉ, and H. KANAMORI (1998), *Computation of seismograms and atmospheric oscillations by normal-mode summation for a spherical Earth model with realistic atmosphere*, Geophys. J. Int., *135*, 388–406.

LOGNONNÉ, P. J., R. ARTRU, F. GARCIA, V. CRESPON, E. DUCIC, G. JEANSOU, J. OCCHIPINTI, G. HELBERT, G. MOREAUX, and P. E. GODET (2006), *Ground based GPS imaging of ionospheric post-seismic signal*, Planet. Space Sci., *54*, 528–540.

MATSUMURA, M., A. SAITO, T. IYEMORI, H. SHINAGAWA, T. TSUGAWA, Y. OTSUKA, M. NISHIOKA, and C. H. CHEN (2011), *Numerical simulations of atmospheric waves excited by the 2011 off the Pacific coast of Tohoku Earthquake*, Earth Planets Space, *63*, this issue, 885–889.

MARUYAMA T., TSUGAWA T., KATO H., SAITO A., OTSUKA Y., NISHIOKA M., (2011), *Ionospheric multiple stratifications and irregularities induced by the 2011 off the Pacific coast of Tohoku Earthquake*. Earth Planets Space, *63*, 69–873.

MÉTOIS, et al., (2013), *Revisiting the North Chile seismic gap segmentation using GPS-derived interseismic coupling*. Geophys. J. Int., *194*, 1283–1294.

NAVA B., RADICELLA S.M., LEITINGER R., COISSON P., (2007), *Use of total electron content data to analyze ionosphere electron density gradients*, Advances in Space Research, *39*, 1292–1297.

OKADA Y., (1992), *Internal deformation due to shear and tensile faults in a half-space*. Bull. Seismol. Soc. Am., *82*(2), 1018–1040.

OCCHIPINTI G., DOREY P., FARGES T., LOGNONNÉ P., (2010), *Nostradamus: The radar that wanted to be a seismometer*. Geophys. Res. Lett., *37*, L18104, doi:10.1029/2010GL044009.

OGAWA T., NISHITANI N., TSUGAWA T., SHIOKAWA K., (2012), *Giant ionospheric disturbances observed with the Super DARN Hokkaido HF radar and GPS network after the 2011 Tohoku earthquake*. Earth Planets Space, *64*, 1295–1307.

OZEKI, M. and K. HEKI (2010), *Ionospheric holes made by ballistic missiles from North Korea detected with a Japanese dense GPS array*, J. Geophys. Res., *115*, A09314, doi:10.1029/2010JA015531.

PULINETS, S. (2004), *Ionospheric precursors of earthquakes; Recent advances in theory and practical applications*, Terr. Atmos. Oceanic Sci., *15*, 413–435.

REDDY, C.D., A.S. SUNIL, G.GONZÁLEZ, MAHESH N.SHRIVASTAVA, MARCOS MORENO (2015), *Near-field co-seismic ionospheric response due to the northern Chile Mw 8.1 Pisagua earthquake on April 1, 2014 from GPS observations*. J. Atmos. Sol. Terr. Phys., *134*, 1–8.

REDDY, C. D., and G. K. SEEMALA (2015), *Two-mode ionospheric response and Rayleigh wave group velocity distribution reckoned from GPS measurement following Mw 7.8 Nepal earthquake on 25 April 2015*. J. Geophys. Res., *120*, doi:10.1002/2015JA021502.

ROLLAND, L. M., P. LOGNONNE, and H. MUNEKANE, (2011), *Detection and modeling of Rayleigh wave induced patterns in the ionosphere*, J. Geophys. Res., *116*, A05320, doi:10.1029/2010JA016060.

ROW R. V., (1967), *Acoustic-gravity waves in the upper atmosphere due to a nuclear detonation and an earthquake*. J. Geophys. Res., *72*, 1599–1610.

SAGIYA T., (2004), *A decade of GEONET: 1994–2003 The continuous GPS observation in Japan and its impact on earthquake studies*. Earth Planets Space, *56*, 29–41.

SAITO A., NISHIMURA M., YAMAMOTO N., et al., (2001), *Traveling ionospheric disturbances detected in the FRONT campaign*. Geophys. Res. Lett., *28*, 689–692.

SAITO, A., TSUGAWA, T., OTSUKA, Y., NISHIOKA, M., IYEMORI, T., MATSUMURA, M., SAITO, S., CHEN, C.H., GOI, Y., and CHOOSAKUL, N., (2011), *Acoustic resonance and plasma depletion detected by GPS total electron content observation after the 2011 off the Pacific coast of Tohoku Earthquake*. Earth Planets Space, *63*, 863–867 (this issue).

SARDÓN, E., and N. ZARRAOA (1997), *Estimation of total electron content using GPS data: How stable are the differential satellite*

*and receiver instrumental biases?*. Radio Sci., *32*(5), 1899–1910, doi:10.1029/97RS01457.

SCHURR et al., (2014), *Gradual unlocking of plate boundary controlled initiation of the 2014 Iquique earthquake*, Nature *512*, 299–302, doi:10.1038/nature13681.

SEEMALA, G. K., and C. E. VALLADARES, (2011), *Statistics of total electron content depletions observed over the South American continent for the year 2008*, Radio Sci., *46*, RS5019, doi:10.1029/2011RS004722.

SUNIL,A.S, MALA S BAGIYA, C.D. REDDY, MANISH KUMAR and D.S. RAMESH, (2015), *Post-seismic ionospheric response to the 11 April 2012 East Indian Ocean doublet earthquake*. Earth, Planets and Space, *67*:37, doi:10.1186/s40623-015-0200-8.

TSAI H. F., LIU J. Y., LIN C. H., CHEN C. H., (2011), *Tracking the epicenter and the tsunami origin with GPS ionosphere observation*. Earth Planets Space, *63*, 859–862.

TODA S., STEIN R. S., RICHARDS-DINGER K., BOZKURT S., (2005), *Forecasting the evolution of seismicity in southern California: Animations built on earthquake stress transfer*. J. Geophys. Res., B05S16, doi:10.1029/2004JB003415.

VALLADARES, C. E., J. VILLALOBOS, M. A. HEI, R. SHEEHAN, S. BASU, E.MACKENZIE, P. H. DOHERTY, and V. H. RIOS (2009), *Simultaneous observation of travelling ionospheric disturbances in the Northern and Southern Hemispheres*. Ann. Geophys., *27*, 1501–1508, doi:10.5194/angeo-27-1501-2009.

YE, L., THORNE LAY, HIROO KANAMORI, and KEITH D. KOPER, (2015), *Rapidly Estimated Seismic Source Parameters for the 16 September 2015 Illapel, Chile Mw 8.3 Earthquake*, Pure and Applied Geophysics, doi:10.1007/s00024-015-1202.